7-2020

Processing-structure-property relationships of biopolyester/zinc oxide fibrous scaffolds engineered by centrifugal spinning

Victoria Padilla-Gainza

Heriberto Rodríguez-Tobías

Graciela Morales

Antonio Ledezma-Pérez

Carmen Alvarado-Canché

See next page for additional authors

Authors

Victoria Padilla-Gainza, Heriberto Rodríguez-Tobías, Graciela Morales, Antonio Ledezma-Pérez, Carmen Alvarado-Canché, Cristobal Rodriguez, Robert Gilkerson, and Karen Lozano

Padilla-Gainza Victoria (Orcid ID: 0000-0002-4676-1337)

Processing-structure-property relationships of biopolyester/zinc oxide fibrous scaffolds engineered by centrifugal spinning

V. Padilla-Gainza[a], H. Rodríguez-Tobías[a*], G. Morales[a*], A. Ledezma-Pérez[a], C. Alvarado-Canché[a], C. Rodríguez[b], R. Gilkerson[b], K. Lozano[c]

[a] Centro de Investigación en Química Aplicada, Blvd. Enrique Reyna 140, Saltillo, CP 25294, Coah., México.
[b] Biology Department, University of Texas Rio Grande Valley, 1201 W University Dr, Edinburg, TX 78539, USA.
[c] Mechanical Engineering Department, University of Texas Rio Grande Valley, 1201 W University Dr. Edinburg, TX 78539, USA.
Graciela.morales@ciqa.edu.mx, lcq.heriberto.rodríguez@gmail.com

Victoria Maria Padilla Gainza
Affiliation: Centro de Investigación en Química Aplicada, Blvd. Enrique Reyna 140, Saltillo, CP 25294, Coah., Mexico.
ORCID: 0000-0002-4676-1337
Mailing Address: 1201 W University Dr. Edinburg TX 78539
e-mail: viquipadilla@gmail.com

Heriberto Rodríguez Tobías
Affiliation: Centro de Investigación en Química Aplicada, Blvd. Enrique Reyna 140, Saltillo, CP 25294, Coah., Mexico.
ORCID: 0000-0001-9608-5843
e-mail: lcq.heriberto.rodriguez@gmail.com

Graciela Morales
Affiliation: Centro de Investigación en Química Aplicada, Blvd. Enrique Reyna 140, Saltillo, CP 25294, Coah., Mexico.
ORCID: 0000-0003-0714-4325
e-mail: graciela.morales@ciqa.edu.mx

Antonio Serguei Ledezma Pérez
Affiliation: Centro de Investigación en Química Aplicada, Blvd. Enrique Reyna 140, Saltillo, CP 25294, Coah., Mexico.
ORCID: 0000-0003-0549-0208
e-mail: Antonio.ledezma@ciqa.edu.mx

Carmen Natividad Alvarado Canché
Affiliation: Centro de Investigación en Química Aplicada, Blvd. Enrique Reyna 140, Saltillo, CP 25294, Coah., Mexico.
ORCID 0000-0002-9193-7239
e-mail: carmen.alvarado@ciqa.edu.mx

Cristóbal Rodríguez
Affiliation: University of Texas Rio Grande Valley, 1201 West University Drive, Edinburg, TX 78539, USA.
ORCID: 0000-0003-1836-1923
e-mail: cristobal.rodriguez01@utrgv.edu

This is the author manuscript accepted for publication and has undergone full peer review but has not been through the copyediting, typesetting, pagination and proofreading process, which may lead to differences between this version and the Version of Record. Please cite this article as doi: 10.1002/pat.4987

Robert Gilkerson
Affiliation: University of Texas Rio Grande Valley, 1201 West University Drive, Edinburg, TX 78539, USA.
ORCID: 0000-0002-5725-6627
e-mail: Robert.gilkerson@utrgv.edu

Karen Lozano
Affiliation: University of Texas Rio Grande Valley, 1201 West University Drive, Edinburg, TX 78539, USA.
ORCID: 0000-0002-6676-8632
e-mail: karen.lozano@utrgv.edu

Processing-structure-property relationships of biopolyester/zinc Oxide fibrous scaffolds engineered by centrifugal spinning

V. Padilla-Gainza[a], H. Rodríguez-Tobías[a*], G. Morales[a*], A. Ledezma-Pérez[a], C. Alvarado-Canché[a], C. Rodríguez[b], R. Gilkerson[b], K. Lozano[c]

[a] Centro de Investigación en Química Aplicada, Blvd. Enrique Reyna 140, Saltillo, CP 25294, Coah., México.

[b] University of Texas Rio Grande Valley, 1201 West University Drive, Edinburg, TX 78539, USA.

[c] Mechanical Engineering Department, University of Texas Rio Grande Valley, 1201 W University Dr. Edinburg, TX 78539, USA.

Graciela.morales@ciqa.edu.mx, lcq.heriberto.rodríguez@gmail.com

Abstract

This study addresses the processing of nonwoven fibrous materials obtained by centrifugal spinning method, namely Forcespinning®; a high yield and low production cost technique little explored in this field. Poly(D, L-lactic acid) (PDLLA) and poly(3-hydroxybutyrate) (PHB) were used as matrices and reinforced with zinc oxide nanoparticles (n-ZnO). The morphology, mechanical, and thermal performance of the developed composites were analyzed as well as the antibacterial effect of n-ZnO. Fibrous materials with n-ZnO concentrations of 1, 3 and 5 wt. % for PDLLA and 1 and 3 wt. % for PHB were evaluated. The results showed that the incorporation of n-ZnO produces an increase in the viscosity of the precursor solutions for both polymeric systems, which caused an increase in the average fiber diameter, though the morphology was not affected, obtaining mostly long, continuous, and homogenous fibers. In addition, a decrease in thermal stability was observed to a greater extent in PDLLA systems. Regarding the mechanical performance, optimal properties were obtained at a concentration of 3 and 1 wt. % of n-ZnO for PDLLA and PHB, respectively. Antibacterial studies showed that PHB with 1 and 3 wt. % of n-ZnO effectively combat strains of *E. coli* and *S. aureus*, presenting 100% of strain growth inhibition. In the case of PDLLA, a higher n-ZnO concentration (5 wt.%) was required to reach a strain growth inhibition above 97%. Finally, cell viability tests demonstrated that the designed fibrous mats support cell proliferation, indicating their potential for use as scaffolds in bone tissue regeneration.

Keywords: Forcespinning; centrifugal spinning; polymeric fibers; zinc oxide; poly(D, L-lactic acid); poly(3-hydroxybutyrate), antibacterial scaffolds

Running head: Processing-structure-property relationships of fibrous scaffolds

1. Introduction

Polymeric fibers have gained interest in the biomedical area given its attractive morphology and similarity with different extracellular matrices. A wide variety of nanofibrous systems have been developed to analyze cell adhesion, growth, and proliferation.[1,2] However, it is important to note that this fiber morphology also presents a platform to the adhesion of pathogenic microorganisms, which could lead to serious infections.[3] The successful performance of these nanofibrous scaffolds is highly dependent on their antibacterial properties.[4–6] Consequently, researchers have focused their attention on the effect of incorporating biocidal agents (antibiotic, organic substances, metals and metal oxides).

There are different metals and metal oxides nanoparticles (NPs), for example, MgO, Ag, Fe_2O_3, TiO_2, CuO, $Mg(OH)_2$ and ZnO, that have been used for biotechnological and biomedical applications. Among the above mentioned metal oxides, zinc oxide nanoparticles (n-ZnO) have shown excellent antimicrobial activity and biocompatibility.[7] Studies have reported that n-ZnO have a selective toxicity for bacteria with minimal effect on human cells.[8] In addition, they have shown to exert an osteoconductive and osteoinductive effect on mesenchymal cells.[9] On the other hand, ZnO nanoparticles have a low production cost, offer simple routes for morphology control, and promote surface interactions with different functional groups.[10,11]

Several studies related to the design of hybrid nanofibers based on biopolyesters and ZnO produced through the electrospinning technique have been published. Specifically, semi-crystalline and amorphous biopolyesters, such as poly(lactic acid) (PLA),[12–15] poly (hydroxyalcanoate)s (PHAs), poly(3-hydroxybutyrate-co-3-hydroxyvalerate) (PHBV),[16–18] and

poly(3-hydroxybutyrate) (PHB), have been reported as matrices suitable for nanofiber development.[19] Regarding the antibacterial performance, the approach has been directed towards strains of clinical interest, such as *E. coli* and *S. aureus*; in this regards, a greater antimicrobial effect of ZnO on *S. aureus* has been observed with a growth inhibition (GI) above 90% at a concentration ≥ 3 wt.% of n-ZnO.[12,14,19]

Despite the academic popularity of the electrospinning technique, it still presents important limitations such as the need of solvents with specific dielectric properties, high energy cost due to the high voltage required, and for basic electrospinning systems, very low production rates ($0.01 mg \cdot h^{-1}$). Although, new methods such as needless electrospinning have shown higher production rates ($10\ g \cdot h^{-1}$)[20] given the multiple jets originated in the drum, though the method is still governed by high electric fields. These constraints have promoted the development of alternative technologies such as centrifugal spinning, drawing, phase separation, self-assembly, template synthesis, freeze-drying synthesis, and interfacial polymerization to mention some. These alternatives circumvent some of the disadvantages of the electrospinning technique.[21] Among the above mentioned technologies, centrifugal spinning (Forcespinning®) is the most competitive when considering potential for commercial use given the high production rate ($50\text{-}100\ g \cdot h^{-1}$)[22] and lower energy costs since there is no need for electric fields. Additionally, the conductivity and/or electrostatic charges of the polymer solution are not relevant parameters for fiber production; therefore, broadening the range of polymers that can be transformed into fibers.[23]

Several studies focused on the design of fibrous materials using centrifugal spinning have been recently reported. Kegan *et al.*[24] produced PHBV membranes functionalized with type I collagen; where the interaction with fibroblast cells showed the potential of these membranes to be used for tissue regeneration. Loordhuswamy *et al*.[25] developed aligned PCL and gelatin fiber mats; through *in vivo* studies, the authors demonstrated the potential of these mats in wound healing applications. Additionally, Jaime and Rogalski in a Rotary Jet Spinning review, reported on several studies that have developed nanofiber systems (from PLA, PCL, polyvinylpyrrolidone (PVP), bacterial

cellulose (BC), crystalline forms of olanzapine, piroxicam and sucrose) for biomedical applications.[26] Despite the increasing number of reports focusing on the design of hybrid materials using centrifugal spinning, the formulation used in this study has not been explored. This opens the possibility of establishing an understanding about the processing-structure-property relationship for n-ZnO reinforced poly(D, L-lactic acid) (PDLLA) and poly(3-hydroxybutyrate) (PHB) nanofiber membranes as well as exploring potential applications of these materials as antibacterial/scaffolds for bone tissue regeneration.

This work reports the development of composite nonwoven fibrous materials, n-ZnO reinforced PDLLA and PHB fibers systems produced by the Forcespinning® technique. The study also presents an analysis of the influence of the n-ZnO nanoparticles on the rheology of the precursor solutions, fiber morphology, and mechanical, thermal and antibacterial performance of the developed nanofibrous systems. Finally, the interaction of the developed systems with osteoblast cells was addressed to assess their potential application as scaffolds for bone tissue regeneration.

2. Experimental Methodology

2.1. Materials and reagents

Poly(D, L-lactic acid) (PDLLA) provided by NatureWorks LLC (Ingeo 6362D) with M_w=160 kg·mol^{-1} and Đ = 1.646, and poly(3-hydroxybutyrate) (PHB) supplied by Goodfellow with M_w= 381 kg·mol^{-1}; Đ = 3.53, were used as polymer matrices. n-ZnO nanoparticles were synthesized through a reaction in methanolic solution assisted by microwave. The solvent used for the polymer solution was chloroform, ACS grade, provided by Fisher Scientific.

2.2. Synthesis of n-ZnO

The synthesis of the n-ZnO was carried out following the procedure described by Rodríguez-Tobías.[27] In a poly(tetrafluoroethylene) (PTFE) reactor, 18 mL of $Zn(CH_3CO_2)_2$ solution (0.32 $mol.L^{-1}$) were added and subjected to vigorous stirring, 54 mL of KOH solution (0.64 $mol.L^{-1}$) were added dropwise. The solutions were prepared using methanol as the solvent. The reaction mixture was placed in a multimodal CEM microwave equipment, model MARS 6, and irradiated for 20 min at 80 °C. The precipitate was subjected to three wash cycles; the first with deionized water and the last two with methanol. Finally, the system was dried in an oven at 70 °C.

Crystallographic structure and chemical analysis were performed by X-ray diffraction (XRD, Siemens model D5000) and FTIR-ATR spectroscopy (Thermo Scientific NICOLET iS50), respectively. The morphology was evaluated by scanning electron (SEM, Carl Zeiss, SigmaVP) and transmission microscopy (TEM, FEI, Titan 80-300). The average particle size was determined by measuring the diameters of 300 particles obtained from several TEM micrographs, using the Image J software version 1.48.

2.3. Preparation of the precursor biopolyester solutions

Dispersions of n-ZnO in chloroform were prepared by using an ultrasound bath (cole-Parmer 8891) for 30 min. Once the dispersion process was completed, the biopolyester was added to the system to obtain the corresponding solution at the established concentration (Table 1). In the case of PDLLA, the solutions were carried out under constant agitation for 22 h at room temperature, while PHB solutions were prepared at a temperature of 55 °C under stirring for 12-16 h.

The viscosities of the biopolyester solutions were determined using an Anton Paar rheometer, physical model MCR 301 with a cone-plate configuration (diameter 50 mm, angle of 2 ° and gap of 0.205) at 25 °C.

2.4. Centrifugal spinning process

The prepared solutions were subjected to a centrifugal spinning process in the Cyclone™ L-1000M (FiberRio Technology, Corp.), which consist of a cylindrical spinneret with two nozzles equipped with regular beveled needles (30-gauge length, Becton, Dickinson and Company) and 8 collectors in the form of metal bars arranged around the spinneret at a distance of 15 cm from the nozzles. For each run, 2 mL of polymer solution were added to the spinneret, and fiber spinning was carried out for a period of 5 min at a temperature of 23 °C ± 3 °C with a relative humidity of 59.3% ± 9.6%. The fibers were placed in a vacuum oven at 30 °C for 24 h, to remove any residual solvent. Finally, the fibers were stored in plastic bags in the presence of a desiccant for moisture control.

2.5. Experimental design

The concentrations of the precursor solutions were established based on the optimization study carried out in a previous work and shown in Table 1.[28] In relation to the angular speed (ω), an adjustment was made taking into account the n-ZnO influence on the rheological behavior of the precursor solutions. Table 1 also lists the intervals of angular velocities (ω) used in the process.

Table 1.- Experimental conditions used during the centrifugal spinning process.

For the selection of the optimum ω, the output variables considered for the evaluation of the fibers were mainly fiber morphology and fiber diameter dispersion. Additionally, the yield/output of the process (ηp) was taken into account according to Equation 1.

$$\eta_P = \frac{M_{mf}}{ST} x100 \qquad (1)$$

where M_{mf} and ST are the grams of fibers collected per run (5 min) and the total solids (polymer + NPs) contained in 2 mL of polymer solution, respectively.

2.6. Fiber characterization

The morphological analysis was carried out using a scanning electron microscope (Carl Zeiss, SigmaVP). The images obtained were analyzed with the Image J software (v. 1.48) to estimate average fiber diameters ($\overline{D_f}$) and average pore size (interfibrillar spaces). Diameter distributions were obtained by measuring 100 fibers (20 fibers per micrograph) with three measurements per fiber, making a total of 300 measurements per sample. Obtained data was represented by means of box-bars charts, where the boxes reflect 50% of the population of values that located between quartile 1 (Q_1 = 25% of the population) and 3 (Q_3 = 75% of the population) and the bars represent the amplitude of the distribution according to the most probable values or those that appear more frequently.

The distribution and dispersion of the n-ZnO within the fibers were determined using energy dispersive X-ray spectroscopy (EDS, EDAX Octane Super) and transmission electron microscopy (FEI, Titan 80-300).

For the calculation of the scaffold's porosity, an adjustment of the equation reported by Wang [29] was used (Equation 2)

$$\emptyset = \left(1 - \frac{m}{Z*A*H*\rho}\right)*100 \qquad (2)$$

Where m, Z, A, H and ρ are the mass, thickness, width, and length of the scaffold and the density of the polymer or mixture of polymer with n-ZnO in the corresponding case, respectively.

The thermal properties were evaluated through thermogravimetric analysis (TGA) (TA Instruments, Q400) and differential scanning calorimetry (DSC) (TA Instruments, Q200). To perform the TGA, the sample was heated from 30 °C to 600 °C under a nitrogen atmosphere, at a heating rate of 10 °C·min^{-1}. Regarding the DSC, the heating was carried out from -70 to 200 °C at a speed of 10 °C·min^{-1}, the sample was isothermally maintained at 200 °C for 2 minutes and then cooled down at the same rate to -70 °C. A second heating cycle under the same conditions was

conducted. The crystallinity of the systems manufactured with PHB was determined using Equation 3:[30]

$$X_c = \frac{\Delta H_m}{\Delta H_m^{\circ} \times X_{PHB}} \times 100 \quad (3)$$

Where ΔH_m and ΔH_m° are the melting enthalpies of the PHB sample and a 100% crystalline PHB respectively, being ΔH_m° = 146 J·g^{-1}. [31] The X_{PHB} is the PHB weight fraction within the sample.

The mechanical properties of the fibrous materials were determined by tensile tests using the universal testing machine (Tinius-Olsen, H10KS). To this end, test pieces of 30 mm long and 3 mm wide were cut and conditioned for 24 h at room temperature (23-25 °C). The tensile test was carried out at a deformation speed of 2 mm·min^{-1} with a clamp separation of 27.5 mm, using a 50 N load cell (5 repetitions).

It is important to mention that the fiber characterization in the optimization stage was determined from the fibers collected from a single run (5 min). Once proper parameters were established, the resultant mats were obtained by the collection of 7-runs (5 min each).

2.7. Antimicrobial properties

The antimicrobial activity of the fibrous materials was evaluated taking as reference the Japanese Industrial Standard, Z280126.[32] The test was performed for two microorganisms of clinical importance, Escherichia coli ATCC-25922 and Staphylococcus aureus ATCC-29213. For the test, 2x2 cm samples under aseptic conditions were inoculated with 4 mL of a microorganism suspension in trypticase soy broth, equivalent to 50000 colony forming units per mL (CFU·mL^{-1}). Subsequently, the samples were incubated at a temperature of 37 °C and 90% humidity for 24 hours. At the end of the incubation time the population of microorganisms present in the samples was determined (the tests were done in quadruplicate), and the antimicrobial activity (*R*) was calculated using Equation 4:

$$R = \left(log\frac{B_t}{B_0} - log\frac{M_t}{B_0}\right) \quad (4)$$

Where B_0 and B_t are the quantities in CFU·mL^{-1} of bacteria that survive in the presence of the blank (material without n-ZnO) before and after 24 hours of incubation, respectively. M_t is the number of bacteria that survive after 24 hours of incubation in the presence of the antimicrobial material (material with n-ZnO). Additionally, inhibition to bacterial growth (GI) was determined by means of Equation 5:

$$GI = \left(\frac{B_t - M_t}{B_t}\right) x100 \quad (5)$$

2.8. Cell viability test

Mouse preosteoblast cells (MC3T3-E1, ATCC) were cultured in a minimum essential medium-α (MEM Alpha-1X, Gibco ™) containing 2.2 g.L^{-1} of $NaHCO_3$, 15% of fetal bovine serum (FBS, Fisher) and 1% of Penicillin-Streptomycin-10,000 U/mL (Gibco ™). 30000 cells in MEM Alpha culture containing serum and penicillin-streptomycin were deposited on PDLLA and PHB mats of 1x1 cm in dimension, the mats had been previously sterilized by 10 min exposure to UV light. After seeding, samples were incubated at 37 °C, under controlled atmosphere with 5% CO_2, for a period of 1, 3, 5 and 7 days. After incubation, cells were rinsed with fresh medium in order to eliminate residue from cell culture. 300 µL of resazurin solution (0.2% w/v, ACROS Organics™) on culture medium (1:10) was then added to the samples and was allowed to react for 4 h. 150 µl were taken from each sample and fluorescence was measured at 570 nm using an iMark™ Microplate Absorbance Reader (BioRad).

3. Results

3.1. Synthesis of n-ZnO

The morphology of n-ZnO and the corresponding particle size distribution and elemental composition can be observed in Figure S1a-b-*Supplementary Information*. The shape of the particles is quasi-spherical with an average diameter of 6.36 ± 2.08 nm. In agreement with results presented in the literature, the obtained morphology is the expected one according to the technique and conditions used for its synthesis.[11,33] EDS analysis reflected the composition to be, Zn and O as 80.54 and 19.45 wt. %, respectively; which is equivalent to a 1:1 molar ratio (Figure S1c-*Supplementary Information*).

The X-ray spectra of the synthesized n-ZnO shows seven well-defined peaks,[34,35] the 2θ values of 31.7 °, 34.5 ° and 36.2 ° can be assigned to the crystalline planes (100), (002) and (101) of the hexagonal phase of ZnO (Figure S1e-*Supplementary Information*). In addition, the amplitude of the signals shows that the size of the ZnO structures is in a nanometric scale according to the average particle diameter ($\overline{D_p}$) determined through TEM micrographs (Figure S1d-*Supplementary Information*).

3.2. Rheological study of the PDLLA or PHB solutions with and without n-ZnO

The apparent viscosity of the polymer solutions was evaluated as a function of the shear rate for 10 and 9 wt. % of PDLLA and PHB, respectively, with and without n-ZnO (Figure 1). In general, no significant influence of shear rate on the systems' viscosity was observed for the analyzed range. In the case of the solutions formulated without NPs, a Newtonian behavior was observed, while the solutions containing 1, 3 and 5 wt. % of n-ZnO exhibited a pseudo-plastic behavior.

Regarding the effect of the n-ZnO on the rheological behavior of the solutions, a dependency of the biopolyester nature was observed. Both systems exhibited, at a particular concentration of NPs, an increase in solution viscosity. In the case of PDLLA solutions, there was a considerable increase in viscosity up to 3 wt. % of ZnO, while at 5 wt. % the viscosity values decreased. On the other hand, PHB solutions showed an increase in viscosity at a concentration of 1 wt. % and above that

concentration, there were no changes. The increase in viscosity suggests a better particle distribution and possible hydrogen bonding interactions between the carboxyl groups of the biopolyester and the hydroxyl groups of the NPs.[36,37]

Figure 1.- Rheological behavior of a) PDLLA solutions at 0, 1, 3 and 5 wt. % of n-ZnO and b) PHB solutions at 0, 1 and 3 wt. % of n-ZnO.

3.3. Effect of n-ZnO on fiber formation

3.3.1. PDLLA

The results show that the concentration of n-ZnO did not have a significant influence on the fiber appearance, fibers are mostly long, continuous, and homogeneous (i.e. no beads are observed) and all exhibited superficial cavities evenly distributed throughout the length of the fiber (Figure S2-*Supplementary Information)*. Similar results were observed by Xuyuan *et al.*[13] with electrospun PLLA fibers, formulated in a concentration range of 0.4 to 2 wt. % of ZnO.

Regarding the $\overline{D_f}$, it was observed that the incorporation of n-ZnO caused an increase of the interval Q_1-Q_3 as well as an extension of its dispersion (Figure S2d-*Supplementary Information*). The fibrous materials containing 1 wt. % of n-ZnO exhibited a Q_1-Q_3 interval of 0.71-1.65 μm while for 3 wt. % and 5 wt. % of n-ZnO the intervals were 0.84-2.06 μm and 1.21-2.48 μm, respectively. These are higher than the results obtained in PDLLA fibers without NPs (0.36-1.08 μm). The resulting fiber morphology corresponds to the obtained rheological behavior of the precursor solutions, as viscosity increases due to the addition of the n-ZnO, the resistance to

elongation increases, resulting in fibers of higher $\overline{D_f}$ at the same angular speed (ω = 9000 rpm).[38,39] The incorporation of NPs also caused changes in the dispersion of fiber diameters.

Taking as reference that fibrous materials with a greater surface area ($\overline{D_f}$ <1 μm)[40] have characteristics that promote cell adhesion and proliferation, the ω that favors the aforementioned morphological characteristics was identified. In this sense, ω was evaluated from 9000 to 11000 rpm, obtaining at 11000 rpm mostly fibers with homogeneous morphologies and diameters displaced towards lower values. It is important to mention that, in most of the systems the production yield was ≥ 60% (Figure S3 and S4-*Supplementary Information*).

3.3.2. PHB

These fibers, mostly had a relatively homogeneous appearance with some bumps and surface irregularities; due not only to the presence of certain n-ZnO agglomerates, but also to the wide molecular weight distribution (Đ = 3.53) within the PHB (Figure S5-*Supplementary Information*).

Regarding the values of $\overline{D_f}$, the addition of 1 wt. % n-ZnO led to a slight increase in diameters in the interval Q_1-Q_3 compared to the system without n-ZnO, from 1.00-1.67 μm to 1.35-2.11 μm. This behavior was attributed to an increase in the viscosity of the precursor solution as observed in the rheological study.

The influence of the angular velocity on the morphology, diameters, and fiber yield was evaluated from 6000 to 9000 rpm. Unlike the PDLLA, the increase of ω did not cause a systematic decrease in fiber diameter. The yield for all tested parameters was above 60%. The systems that presented homogeneous fibers and a displacement of the Q_1-Q_3 interval towards smaller diameters were obtained at 7000 rpm. (Figure S6 and S7-*Supplementary Information*)

3.4. Morphological, thermal, mechanical and antibacterial characteristics of the centrifugal spun materials manufactured with PDLLA-ZnO and PHB-ZnO

3.4.1. Morphology of PDLLA-ZnO systems

In Figure 2, SEM images of the fibrous materials obtained at 1, 3 and 5 wt. % of n-ZnO are shown. In these systems, a correlation with the optimization process is observed regarding the homogeneity and surface morphology of the fibers, as well as fiber diameter distributions (Figure S2 and S3, *Supplementary Information*).

Figure 2.- SEM images of PDLLA fibrous material at 1 wt. % (a and b), 3 wt. % (d and e) and 5 wt. % (g and h) of ZnO, box charts of fiber diameters and porosities (Ø) (c, f and i).

The distribution of NPs within the fibers is observed in Figure 3b, e and h (points in the elemental mapping images). It can be observed that as n-ZnO concentration increases, the presence of some agglomerates becomes apparent. These results were corroborated by TEM images, in which it can be seen a quite homogeneous distribution at low n-ZnO concentration (1 wt. %), with agglomerates ranging from 10 nm to 200 nm (Figure 3c). In the case corresponding to 3 wt. % (Figure 3f) and 5 wt. % (Figures 3g-i) of n-ZnO, the agglomerates have sizes that vary in the range of 10 to 450 nm and 15 to 500 nm, respectively. Taking into account that $\overline{D_p}$ of n-ZnO is 6.36 ± 2.08 nm, the agglomerates are relatively large.

The scaffolds' porosity (spaces between fibers, Figures 2c, f and i), calculated under the considerations described in section 2.6, is greater than 90%. Additionally, through the Image J software, the area distribution between fibers was determined and it was found that approximately 50% of the areas have a dimension/size above 35 ± 10.5 μm^2 and most of the values are distributed over a range from 2 to 200 μm^2. These results show that the pores have sizes large enough to guarantee cellular migration (Figure S8-*Supplementary Information*).[41]

Figure 3.- SEM images (a, d and g), elemental mapping of zinc (b, e and h) and TEM images (c, f and i) of PDLLA fibrous material at 1 wt. % (a, b and c), 3 wt. % (d, e and f) and 5 wt. % (g, h and i) of n-ZnO (images obtained by SEM-EDS).

3.4.2. Morphology of PHB-ZnO systems

In Figure 4, SEM images of PHB fibers containing 1 wt. % (a and b) and 3 wt. % (d and f) of n-ZnO are presented. In these images, the characteristic irregularities of the fibers with their rough surface morphology can be appreciated. In general terms, the fiber surface appearance is heterogeneous and depends on the fiber thickness; behavior that can be better appreciated at a concentration of 3 wt. % of n-ZnO. Unlike the PDLLA, the dispersion of fiber diameters of both systems showed significant variations in comparison with the dispersion obtained in the optimization phase (Figure S7-*Supplementary Information*).

As observed for PDLLA system, the presence of some agglomerates was also evident (Figure 5b and e). Through the analysis of several TEM images, it was determined that the sizes of the agglomerates fluctuated from 15 to 140 nm and 15 to 800 nm at a concentration of 1 and 3 wt. % n-ZnO, respectively (Figure 5c and 5f). With these results, a strong tendency of n-ZnO to form aggregates was evidenced mainly due to the NP's size and possibly to a lesser interaction with the polymeric matrix, in comparison to PDLLA.

The porosities (Figure 4c and f) and the pore sizes in the scaffolds were found to be similar to those observed in PDLLA (Figure S9-*Supplementary Information*).

Figure 4.- SEM images of PHB fibrous material at 1 wt. % (a and b) and 3 wt. % (d and e) of n-ZnO, box charts of fiber diameters and porosities (Ø) (c and f).

Figure 5.- SEM images (a and d), elemental mapping of n-zinc (b and e) and TEM images (c and f) of PHB fibrous material at 1 wt. % (upper images) and 3 wt. % (bottom images) of n-ZnO (images obtained by SEM-EDS).

3.4.3. Thermal properties of PDLLA-ZnO systems

In Figure 6a, the thermo-degradation patterns of the materials formulated at different concentrations of n-ZnO are presented. In the first instance, it is evident that the residues after the heat treatment slightly disagree with the original n-ZnO concentration (1.1, 2.4 and 3.8 wt. %, for 1, 3 and 5 wt. %, respectively). These results could suggest a non-homogeneous distribution of NPs derived from their tendency to form agglomerates, losses of NPs during the fiber production process, or a combination of both.

For thermal stability, the temperature at which the degradation rate reaches its maximum value (T_d), obtained by means of the derivative of the thermogram, was taken as the reference. The T_d of the materials containing 0, 1, 3 and 5 wt. % of n-ZnO were 362, 291, 277 and 274 °C, respectively (Figure S10, *Supplementary Information*). It is evident that ZnO promoted a decrease in the thermal stability of the polymer, showing a more pronounced effect at a concentration of 1 wt. %. Different publications attribute this behavior to the fact that ZnO promotes reactions of transesterification and depolymerization of PLA.[42–45] At 3 and 5 wt. % of n-ZnO concentration there were no significant changes in the degradation temperatures, possibly due to the agglomerates of n-ZnO, which cause a decrease in the available active sites and therefore less interaction with polymer chains.[44]

Concerning the thermal transitions of the materials, in Figure 7a the DSC thermograms of one heating-cooling-heating cycle are presented. Regarding the reference system (without n-ZnO), in the first heating, an endothermic transition can be observed at 64.9 °C, which occurs just after the glass transition temperature (T_g) of the PDLLA (62.0 °C) (Table 1, *Supplementary Information)*. This behavior denotes the presence of certain arrangement within the polymer chains formed by

the uniaxial stretching experienced during the spinning process. A similar behavior was observed at 1, 3 and 5 wt. % of n-ZnO, but in these cases the endothermic peak occurred at a slightly lower temperature, with a progressive decrease in the enthalpies of relaxation as the concentration of NPs increased. These results indicate that in the process of elongation of the polymeric fluid, the NPs interfere with the alignment of the polymeric chains, leading to a lower structural order. On the other hand, during the cooling cycle and second heating, after polymer chain relaxation, only a second order transition (T_g), typical of an amorphous polymer was observed, as expected.

3.4.4. Thermal properties of PHB-ZnO systems

The TGA thermograms corresponding to the PHB fibers containing 1 and 3 wt. % of n-ZnO (Figure 6b) reflect concentrations closer to the established values, being 1.4 and 3.4%, respectively. It is important to note that although the PHB has a thermal stability lower than that of PDLLA, n-ZnO did not show a pronounced effect on the degradation temperature of the material, which agrees with that reported by Anz Lovar *et al*.[43] who carried out a study of the thermal degradation of PLA-ZnO and PHVB-ZnO, and showed that the metal oxide of interest degrades PLA to a greater extent. The T_d of the materials formulated at 0, 1 and 3 wt. %, were 272, 267 and 264 °C, respectively (Figure S10, *Supplementary Information).*

Figure 7b shows the DSC thermograms of the heating-cooling-heating cycle. Taking as a basis that the PHB used is composed of 95% poly(3-hydroxybutyrate) (3-PHB), 4% poly(4-hydroxybutyrate) (4-PHB) and 1% polyhydroxyvalerate (3-PHV), composition obtained through ^{13}C NMR (Figure S11, *Supplementary Information*), in the first heating two endothermic peaks at 48 °C and 170 °C were identified, corresponding to the fusion of the crystalline phases of the 4-PHB and 3-PHB, respectively. [46] The n-ZnO caused a slight decrease in the percentage of polymer crystallinity, being 47.5, 46.6 and 45.2 wt. % at 0, 1 and 3 wt. % of n-ZnO, respectively. In the cooling process a reduction of the temperature and enthalpy of crystallization occurred when the concentration of n-ZnO increased. This behavior indicates that the n-ZnO NPs are delaying the

crystallization process of the polymer, possibly because they interfere with the packing of the polymer chains, in a similar way to that observed in PHBV-ZnO systems.[18] In the second heating process, two fusion transitions appear with the addition of n-ZnO, which may be related to compositional heterogeneity, multiple crystalline forms, or a fusion-recrystallization-fusion process (Table S2-*Supplementary Information*).

Figure 6.- Degradation patterns derived from TGA of the centrifugally spun PDLLA fibers (a) and PHB fibers (b) obtained at different concentrations of n-ZnO.

Figure 7.- DSC thermograms derived from one cycle of heating-cooling-heating of a) PDLLA and b) PHB fibrous mats at different concentration of n-ZnO.

3.4.5. Mechanical properties of PDLLA-ZnO and PHB-ZnO systems

In Figure 8a the Young's modulus (E) and the tensile strength (σ) of PDLLA materials are plotted as a function of n-ZnO concentration. The results show that for the 1 wt. % sample, there is no influence of n-ZnO on the mechanical performance of the materials, while at 3 wt. % an effect is observed (E = 32.24 MPa, σ = 0.878 MPa) attributed to the stiffening of the material by the interaction of the n-ZnO with the polymeric matrix. When increasing the concentration to 5 wt. % of n-ZnO there was a considerable decrease in tensile strength (E = 5.06 MPa, σ = 0.155 MPa), which is attributed to the presence of agglomerates, which act as stress concentrators and crack initiators.[13,14]

On the other hand, the mechanical performance of PHB materials with and without n-ZnO, is presented in Figure 8b. At a concentration of 1 wt. %, the incorporation of n-ZnO improved the mechanical properties of the material, reflecting a more pronounced effect on the σ. At a concentration of 3 wt. %, no significant changes were observed in the properties (E = 8.985 MPa, σ = 0.643 MPa).

Figure 8.- Young's modulus (E) and tensile strength (σ) of the materials obtained with PDLLA (a) and PHB (b) at different concentrations of n-ZnO.

3.4.6. Antibacterial properties of PDLLA-ZnO and PHB-ZnO

To evaluate the antibacterial effect of the developed materials, a study was carried out with bacteria of clinical interest such as *E. coli* and *S. aureus*. In Table 2, the antibacterial efficiency is presented. In the case of PDLLA, at a concentration of 5 wt. %, an inhibition of bacterial growth for both strains exceeded 97%. On the other hand, the PHB showed an excellent antibacterial performance against both microorganisms, observing a slightly higher efficiency at a concentration of 1 wt. %.

Table 2.- Antimicrobial activity (*R*) and bacterial growth inhibition (*GI*) of the fibrous materials based on PDLLA and PHB at different concentrations of n-ZnO.

3.4.7. Cell viability test

The cell viability test employs resazurin to evaluate cellular metabolic activity. Resazurin displays weak fluorescence under basal conditions. In mammalian cells, mitochondria are maintained as an organellar network responsible for the bulk of bioenergetic metabolism. Within the mitochondria of metabolically-active cells, resazurin is reduced by NADH dehydrogenase, Complex I of the mitochondrial respiratory chain, to produce resorufin, which displays strong fluorescence with a peak ~570-590 nm. Resorufin is excreted into the surrounding media, providing an effective indicator of cellular metabolic activity.[47]

In Figure 9, the viability of the designed scaffolds without (blank) and with n-ZnO for both polymers is shown in relation to the positive control (Ctrl.+, cells alone). Regarding the influence of polymer nature, PDLLA scaffolds promotes greater metabolic activity than PHB scaffolds, with

viabilities above 80%: at days 5 and 7, PDLLA-grown cells displayed resorufin fluorescence equivalent or greater than controls, while PHB-grown cells showed less resorufin fluorescence than control cells. In addition, it was observed that after day 5, an increase in cell viability occurs for both systems. This suggests an adaptation period to the nanofiber environment during the first three days, followed by increased growth and proliferation on subsequent days resulting in increased resorufin signal. In addition, resorufin signal was observed above 100% by PDLLA scaffolds, suggesting that the positive control cells were close to their confluence; therefore, there were no significant changes in their metabolic activity for days 5 and 7. In contrast, PDLLA scaffolds, due to a greater surface area and adequate pore size distribution, allowed cells to continue proliferating. Finally, no statistically significant changes were observed between the cells grown on fibers with and without n-ZnO, demonstrating the ZnO concentrations employed do not have cytotoxic effects on MC3T3 preosteoblast cells as assayed.

Figure 9.- Osteoblast cell viability evaluated after 1, 3, 5 and 7 days with resazurin for PDLLA (a) and PHB (b). A statistical analysis is shown measuring the standard deviation of the mean, n= 3 trial experiment (* $p < 0.05$, ** $p < 0.01$).

4. Discussion

Three-dimensional arrangement of polymeric fibers in a structure of interconnected pores, obtained by different spinning techniques,[12–18] has allowed the design of scaffolds with potential use in the regeneration of different extracellular matrices.[1,2] Zinc oxide reinforced PDLLA and PHB nanofibrous membranes were developed using the Forcespinning® technique, results showed high yields and potential to be use as scaffolds for biomedical applications.

As it was observed in Figures 1, S2 and S3, the viscosity of the precursor solution has an influence on the fiber diameters. In this sense, it is necessary to consider that in the process of uniaxial stretching of a polymeric fluid the molecules are forced to align in the direction of the applied

stress. However, when the fluid has an elastic behavior and high viscosity, it presents a certain resistance to be elongated and the aligned chains tend to relax to assume their original non-aligned conformation, producing larger fiber diameters distributed in a wider range of values.[48] This effect was evidenced to a great extent in PDLLA systems.

On the other hand, the polymer chain entanglements have an important role in the homogeneous fiber formation. It was previously reported for a PDLLA system that the conditions under which it is possible to obtain homogeneous fibers by means of Forcespinning® were 10 wt. % polymer solution and ω = 9000 rpm.[28] According to Chae *et al.*[49] the incorporation of n-ZnO would reinforce the polymer chain entanglements, as a consequence of an increase in interfacial polymer-nanoparticle interaction. Even though the presence of n-ZnO did not produce a significant effect on the fiber appearance, its influence on the chain entanglement was reflected on the mechanical performance.

As evidenced in Figure 6, n-ZnO caused a decrease in the thermal stability of the materials, with a pronounced effect in PDLLA systems. Based on a study conducted by Anzlovar *et al*. [38] ZnO catalyzes and forms part of the degradation reactions of PLA and PHBV, with a minor effect on PHBV. Figure 7a shows a slight decrease in the T_g of PDLLA, results consistent with the observed decrease in thermal stability. In the case of PHB (Figure 7b) the decrease in the T_m and the percentage of crystalline phase observed in the first heating suggests that n-ZnO had some influence on the lamellar structure of the polymer[50] and it acts as a retardant agent of crystallization. These results are in agreement with the decrease in the crystallization temperatures observed during the cooling phase. Finally, in relation to the second heating, the presence of n-ZnO could have caused the crystallization of a secondary phase (less stable) during the cooling process, which melts at a lower temperature (157 °C, first melting peak), crystallizes and melts again at a higher temperature (167.3 °C, second melting peak) (Table 2-*Supplementary Information*).[18]

Comparatively, the materials based on PDLLA presented a better mechanical performance except for the system containing 5 wt. % of n-ZnO which showed large aggregates (Figure 3h-i). These aggregates diminished the concentration/number of active sites due to particle-matrix interactions while also act as stress concentrators promoting the failure of the material. Size and dispersion of the nanoparticles played a key role on mechanical performance.

Concerning the antibacterial performance of the designed scaffolds, it was observed that there was a difference in the sensitivity of the strains and required n-ZnO concentration to combat the strains. Lower concentrations of n-ZnO (1 and 3 wt. %) show, a greater sensitivity of *S. aureus* to PDLLA scaffolds. These results are in agreement with those reported by Sirelkhatim *et al.*[51] and Reddy *et al.*,[52] where the growth inhibition *of S. aureus* bacteria (gram-positive) occurs at a lower n-ZnO concentration compared to *E. coli* bacteria (gram-negative). This behavior is attributed to variations in cell physiology, cell wall constitution and metabolism of the two strains.[51]

Overall, PHB-ZnO fiber systems showed a better performance than PDLLA-ZnO against any of the analyzed strains. In the case of PDLLA, unlike the PHB, a greater interaction between n-ZnO and polymeric matrix was observed (see section 3.2), producing fibers with a high number of embedded NPs; characteristic that harms the material antibacterial properties as it was observed. These results agree with results observed by Virovska *et al.*[12] and Rodríguez-Tobías *et al.*[14] who were working with the effect to electrospinning/electrospraying and electrospinning techniques on the antibacterial performance of PLA fibrous material. They found that the incorporation of ZnO through the polymer solution it was not sufficient to produce a good antimicrobial performance of PLA. The concentration of n-ZnO necessary to inhibit bacteria growth above 95% was determined for PDLLA and PHB, as 0.1 mg/mL and 0.05 $mg \cdot mL^{-1}$, respectively. In the case of PHB, Rodríguez-Tobías *et al.*[19] reported a concentration of 0.09 $mg \cdot mL^{-1}$, which is an approximate value to the one estimated in this study.

Finally, it was demonstrated that PLA and PHB fibers support the growth of mammalian cells (mc3T3 murine preosteoblasts). The cell viability study showed that PDLLA scaffolds presented a better performance than PHB scaffolds. This could be attributed to the larger surface area (fiber diameter distributions more displaced towards lower values, greater surface roughness and spaces between fibers) shown in the PDLLA fiber mats.[41,53] As mentioned above, the concentration of n-ZnO did not show a significant effect on the osteoblast cell viability. Similar results have been presented by Khader and Arinzeh when studying human mesequimal cell proliferation in policaprolactone/ZnO fibrous mats.[54] However, several reports based on ZnO hybrid fibrous materials have presented a decrease on cell viability as ZnO concentration increases.[13,55] Therefore, complementary studies as osteogenic diferenciation and alkaline phosphatase activity could help to further understand the effect of ZnO on cell behavior. [56]

5. Conclusions

The incorporation of n-ZnO produced an increase in the viscosity of PDLLA and PHB precursor solutions, with a greater impact on PDLLA, resulting in an increase of average fiber diameter. The overall morphology was not affected by the presence of n-ZnO, fibers were in both cases, mostly long, continuous and homogeneous. The thermal stability decreases due to the presence of n-ZnO, to a greater extent in PDLLA systems, possibly due to the catalytic effect and higher interaction of the NPs with the PDLLA matrix. In the case of PHB, the incorporation of n-ZnO did not present a significant effect in its thermal stability. Mechanical evaluation showed an increase in Young's modulus and tensile strength at a concentration of 3 wt. % and 1 wt. % for PDLLA and PHB, respectively. For antibacterial applications, the mats produced with PHB at 1 and 3 wt. % of n-ZnO presented an excellent alternative against both *E. coli* and *S. aureus*. In the case of PDLLA, a concentration of 5 wt. % of n-ZnO was required to observe antibacterial activity greater than 97%. As for osteoblast cell viability, the PDLLA scaffolds provided better performance to be used for bone tissue regeneration.

6. Acknowledgments

The authors would like to thank Consejo Nacional de Ciencia y Tecnología (CONACYT, México) for providing V. Padilla Gainza with a Ph.D. grant as well as financial support for her research stay at the University of Texas Rio Grande Valley (UTRGV, Edinburg, Texas). The authors would also like to thank Enrique Jiménez (CIQA, Saltillo, México) for the facilities related to viscosity measurements, Anabel Ochoa (CIQA) for their technical support in the evaluation of the thermal properties (TGA and DSC), and Alejandro Castillo (UTRGV) and Esmeralda Monserrat Saucedo (CIQA) for their technical assistance in electron microscopy characterization. The authors also acknowledge support received from National Science Foundation under PREM grant DMR 1523577.

7. References

1. Jun I, Han HS, Edwards JR, Jeon H. Electrospun fibrous scaffolds for tissue engineering: Viewpoints on architecture and fabrication. *Int J Mol Sci*. 2018;19(3). doi:10.3390/ijms19030745

2. Bhattarai DP, Aguilar LE, Park CH, Kim CS. A review on properties of natural and synthetic based electrospun fibrous materials for bone tissue engineering. *Membranes*. 2018;8(3). doi:10.3390/membranes8030062

3. Gao Y, Truong YB, Zhu Y, Louis Kyratzis I. Electrospun antibacterial nanofibers: Production, activity, and in vivo applications. *J Appl Polym Sci*. 2014;131(18):9041-9053.

4. Cho O-H, Bae I-G, Moon SM, Park S-Y, Kwak Y-G, Kim B-N, Yu S-N, Jeon M-H, Kim T, Choo E-Ju, Lee E-J, Kim T-H, Choi S-H, Chung J-W, Kang K-C, Lee J-H, Lee Y-M, Lee M-S, Park K-H. Therapeutic outcome of spinal implant infections caused by Staphylococcus aureus. *Medicine*. 2018;97(40). doi:10.1097/MD.0000000000012629

5. Ribeiro M, Monteiro FJ, Ferraz MP. Infection of orthopedic implants with emphasis on bacterial adhesion process and techniques used in studying bacterial-material interactions. *Biomatter*. 2012;2(4):176-194.

6. Moriarty F, Kuehl R, Coenye T, Metsemakers W-J, Morgenstern M, Schwarz E, Riool M,

Zaat S, Khana N, Kates S, Richards G. Orthopaedic device-related infection: current and future interventions for improved prevention and treatment. *EFORT Open Rev*. 2016;1(2):89-99.

7. Gnaneshwar PV, Sudakaran SV, Abisegapriyan S, et al. Ramification of zinc oxide doped hydroxyapatite biocomposites for the mineralization of osteoblasts. *Mater Sci Eng C*. 2019;96(August 2018):337-346.

8. Xie Y, He Y, Irwin PL, Jin T, Shi X. Antibacterial activity and mechanism of action of zinc oxide nanoparticles against Campylobacter jejuni. *Appl Environ Microbiol*. 2011;77(7):2325-2331.

9. Yusa K, Yamamoto O, Takano H, Fukuda M, Iino M. Zinc-modified titanium surface enhances osteoblast differentiation of dental pulp stem cells in vitro. *Sci Rep*. 2016;6(April):1-11.

10. Rajan Unnithan A, Arthyram R., Sang Kim C. Scaffolds with Antibacterial Properties. In: Thomas S, Grohens Y, Neethu N, eds. *Nanotechnology Applications for Tissue Engineering*. United States of America: Elsevier; 2015:103-104.

11. Barreto GP, Morales G, Quintanilla MLL. Microwave Assisted Synthesis of ZnO Nanoparticles: Effect of Precursor Reagents, Temperature, Irradiation Time, and Additives on Nano-ZnO Morphology Development. *J Mater*. 2013;2013(1):1-11.

12. Virovska D, Paneva D, Manolova N, Rashkov I, Karashanova D. Electrospinning/electrospraying vs. electrospinning: A comparative study on the design of poly(l-lactide)/zinc oxide non-woven textile. *Appl Surf Sci*. 2014;311:842-850.

13. Ji X, Wang T, Guo L, Xiao J, Li Z, Zhang L, Deng Yan, He N. Effect of nanoscale-ZnO on the mechanical property and biocompatibility of electrospun poly(L-lactide) acid/nanoscale-ZnO mats. *J Biomed Nanotechnol*. 2013;9(3):417-423.

14. Rodríguez-Tobías H, Morales G, Ledezma A, Romero J, Grande D. Novel antibacterial electrospun mats based on poly(D,L-lactide) nanofibers and zinc oxide nanoparticles. *J Mater Sci*. 2014;49(24):8373-8385.

15. Huang Y, Wang T, Zhao X, Wang X, Zhou Lu, Yang Y, Liao F, Ju Y. Poly (lactic acid)/ graphene oxide – ZnO nanocomposite films with good mechanical , dynamic mechanical , anti-UV and antibacterial properties. *J Chem Technol Biotechnol*. 2015;90:1677-1684.

16. Hussain SY, Yu HY, Wang D, Yao J. Electrospun poly(3-hydroxybutyrate-co-3-hydroxy-valerate)/cellulose reinforced nanofibrous membranes with ZnO nanocrystals for antibacterial wound dressings. *Cellulose*. 2017;24(7):2925-2938.

17. Naphade R, Jog J. Electrospinning of PHBV/ZnO membranes: Structure and properties. *Fibers Polym*. 2012;13(6):692-697.

18. Yu W, Lan CH, Wang SJ, Fang PF, Sun YM. Influence of zinc oxide nanoparticles on the crystallization behavior of electrospun poly(3-hydroxybutyrate-co-3-hydroxyvalerate) nanofibers. *Polymer*. 2010;51(11):2403-2409.

19. Rodríguez-Tobías H, Morales G, Ledezma A, Romero J, Saldívar R, Langlois V, Renard E, Grande D. Electrospinning and electrospraying techniques for designing novel antibacterial poly(3-hydroxybutyrate)/zinc oxide nanofibrous composites. *J Mater Sci*. 2016;51(18):8593-8609.

20. Persano L, Camposeo A, Tekmen C, Pisignano D. Industrial upscaling of electrospinning and applications of polymer nanofibers: A review. *Macromol Mater Eng*. 2013;298(5):504-520.

21. Alghoraibi I., Alomari S. (2018) Different Methods for Nanofiber Design and Fabrication. In: Barhoum A., Bechelany M., Makhlouf A. (eds) Handbook of Nanofibers. Springer, Cham.

22. Sebe I, Szabó B, Nagy ZK, Szabó D, Zsidai L, Kocsis B, Zelkó R. Polymer structure and antimicrobial activity of polyvinylpyrrolidone-based iodine nanofibers prepared with high-speed rotary spinning technique. *Int J Pharm*. 2013;458(1):99-103.

23. Sarkar K, Gomez C, Zambrano S, Ramirez M, Hoyos E, Vasquez H, Lozano K. Electrospinning to Forcespinning. *Materialstoday*. 2010;13(11):13-15.

24. McColgan-Bannon K, Upson S, Gentile P, Russell S, Dalgarno K, Ferreira A. Biomimetic properties of force-spun PHBV membranes functionalised with collagen as substrates for biomedical application. *Coatings*. 2019;9(6). doi:10.3390/coatings9060364

25. Loordhuswamy AM, Krishnaswamy VR, Korrapati PS, Thinakaran S, Rengaswami GDV. Fabrication of highly aligned fibrous scaffolds for tissue regeneration by centrifugal spinning technology. *Mater Sci Eng C*. 2014;42:799-807.

26. Rogalski JJ, Bastiaansen CWM, Peijs T. Rotary jet spinning review–a potential high yield future for polymer nanofibers. *Nanocomposites*. 2017;3(4):97-121.

27. Rodríguez Tobías H. Nuevos Materiales Híbridos Basados en Poliésteres Biodegradables y Nanopartículas de ZnO: Propiedades Antibacterianas y Protección UV. Centro de Investigación en Químca Aplicada (CIQA). 2015.

28. Padilla-Gainza V, Morales G, Rodríguez-Tobías H, Lozano K. Forcespinning technique for

the production of poly(d,l-lactic acid) submicrometer fibers: Process–morphology–properties relationship. *J Appl Polym Sci*. 2019;136(22):1-9.

29. Wang Z, Zhao C, Pan Z. Porous bead-on-string poly(lactic acid) fibrous membranes for air filtration. *J Colloid Interface Sci*. 2015;441:121-129.

30. Lopresti F, Carfì Pavia F, Vitrano I, Kersaudy-Kerhoas M, Brucato V, La Carrubba V. Effect of hydroxyapatite concentration and size on morpho-mechanical properties of PLA-based randomly oriented and aligned electrospun nanofibrous mats. *J Mech Behav Biomed Mater*. 2020;101(July 2019):103449. doi:10.1016/j.jmbbm.2019.103449

31. Jacquel N, Lo C-W, Wu H-S, Wei Y-H, Wang SS. Solubility of Polyhydroxyalkanoates by Experiment and Thermodynamic Correlations. *AIChE J*. 2007;53(10):2704-2714.

32. Japanese Industrial Standard (Z 2801). Test for antimicrobial activity and efficacy. 2001.

33. Rodríguez-Tobías H, Morales G, Olivas A, Grande D. One-Pot Formation of ZnO-graft-Poly(d, l -Lactide) Hybrid Systems via Microwave-Assisted Polymerization of d, l -Lactide in the Presence of ZnO Nanoparticles. *Macromol Chem Phys*. 2015;216(15):1629-1637.

34. Javed Akhtar M, Ahamed M, Kumar S, Majeed Khan M, Ahmad J, Alrokayan S a. Zinc oxide nanoparticles selectively induce apoptosis in human cancer cells through reactive oxygen species. *Int J Nanomedicine*. 2012;7:845-857.

35. Khorsand Zak a., Razali R, Abd Majid WH, Darroudi M. Synthesis and characterization of a narrow size distribution of zinc oxide nanoparticles. *Int J Nanomedicine*. 2011;6(1):1399-1403.

36. Rokbani H, Ajji A. Rheological Properties of Poly (lactic acid) Solutions Added with Metal Oxide Nanoparticles for Electrospinning. *J Polym Environ*. 2018;26(6):2555-2565.

37. Díez-pascual AM, Díez-vicente AL. Poly (3-hydroxybutyrate)/ ZnO Bionanocomposites with Improved Mechanical , Barrier and Antibacterial Properties. 2014:10950-10973.

38. Hong X, Edirisinghe M, Mahalingam S. Beads, beaded-fibres and fibres: Tailoring the morphology of poly(caprolactone) using pressurised gyration. *Mater Sci Eng C*. 2016;69:1373-1382.

39. Adam M, Delsanti M. Viscosity of semi-dilute polymer solutions. *J Phys*. 1982;43(3):549-557.

40. Christopherson GT, Song H, Mao HQ. The influence of fiber diameter of electrospun substrates on neural stem cell differentiation and proliferation. *Biomaterials*. 2009;30(4):556-564.

41. Porter JR, Ruckh TT, Popat KC. Bone tissue engineering: A review in bone biomimetics and drug delivery strategies. *Biotechnol Prog*. 2009;25(6):1539-1560.

42. Rodríguez-Tobías H, Morales G, Grande D. Improvement of mechanical properties and antibacterial activity of electrospun poly(D,L-lactide)-based mats by incorporation of ZnO-graft-poly(D,L-lactide) nanoparticles. *Mater Chem Phys*. 2016;182:324-331.

43. Anžlovar A, Kržan A, Žagar E. Degradation of PLA/ZnO and PHBV/ZnO composites prepared by melt processing. *Arab J Chem*. 2017. doi.org/10.1016/j.arabjc.2017.07.001.

44. Murariu M, Doumbia A, Bonnaud L, Dechief A, Paint Yo, Ferreira M, Campagne C, Devaux E, Dubois P. High-performance polylactide/ZnO nanocomposites designed for films and fibers with special end-use properties. *Biomacromolecules*. 2011;12(5):1762-1771.

45. Abe H, Takahashi N, Kim KJ, Mochizuki M, Doi Y. Thermal degradation processes of end-capped poly(L-lactide)s in the presence and absence of residual zinc catalyst. *Biomacromolecules*. 2004;5(4):1606-1614.

46. Saito Y, Nakamura S, Hiramitsu M, Doi Y. Microbial Synthesis and Properties of Poly(3-ydroxybutyrate-co-4-hydroxybutyrate). *Polym Int*. 1996;39:169-174.

47. Riss TL, Moravec RA, Niles AL, Niles A, Duellman S, Benink H, Worzella T, and Minor L. Cell Viability Assays. *Assay Guid Man*. 2004:1-25. https://www.ncbi.nlm.nih.gov/books/NBK144065/.

48. Oliveira J, Brichi GS, Marconcini JM, Mattoso LHC, Glenn GM, Medeiros ES. Effect of solvent on the physical and morphological properties of poly(lactic acid) nanofibers obtained by solution blow spinning. *J Eng Fiber Fabr*. 2014;9(4):117-125.

49. Chae DW, Kim BC. Effects of interface affinity on the rheological properties of zinc oxide nanoparticle-suspended polymer solutions. *Macromol Res*. 2010;18(8):772-776.

50. Perez M. Gibbs-Thomson effects in phase transformations. *Scr Mater*. 2005;52(8):709-712.

51. Sirelkhatim A, Mahmud S, Seeni A, et al. Review on zinc oxide nanoparticles: Antibacterial activity and toxicity mechanism. *Nano-Micro Lett*. 2015;7(3):219-242.

52. Reddy KM, Feris K, Bell J, Wingett DG, Punnoosea A. Selective toxicity of zinc oxide nanoparticles to prokaryotic and eukaryotic systems. *appl Phys Lett*. 2015;27(3):320-331.

53. Kumbar SG, James R, Nukavarapu SP, Laurencin CT. Electrospun nanofiber scaffolds: engineering soft tissues. *Biomed Mater*. 2008;3:1-15.

54. Khader A, Arinzeh TL. Biodegradable zinc oxide composite scaffolds promote osteochondral differentiation of mesenchymal stem cells. *Biotechnol Bioeng*. 2020;117(1):194-209.

55. Sánchez F-B, Socci M-A, Sappia M-I, Gómez L-D, Felice M-K, Martí C-J, Pividori M, Simonelli M-I, Rodríguez G, Controlled degradability of PCL-ZnO nanofibrous scaffolds for bone tissue engineering and their antibacterial activity. *Mater Sci Eng C*. 2018;93:724-738.

56. Albrektsson T, Johansson C. Osteoinduction, osteoconduction and osseointegration. *Eur Spine J*. 2001;10:S96-S101.

Table 1.- Experimental conditions used during the centrifugal spinning process.

	C_p (wt. %)	ω (rpm)	C_{NPs} (wt. %)	Identification
PDLLA	10	9000-11000	1	PDLLA-ZnO 1%
			3	PDLLA-ZnO 3%
			5	PDLLA-ZnO 5%
PHB	9	6000-9000	1	PHB-ZnO 1%
			3	PHB-ZnO 3%

*ω= angular speed, C_p = polymer concentration and C_{NPs} = nanoparticles concentration

Table 2.- Antimicrobial activity (*R*) and bacterial growth inhibition (*GI*) of the fibrous materials based on PDLLA and PHB at different concentrations of n-ZnO.

	Escherichia coli				*Staphylococcus aureus*			
	PDLLA		**PHB**		**PDLLA**		**PHB**	
ZnO (wt. %)	**GI (%)**	**R**	**GI (%)**	**R**	**GI (%)**	**R**	**GI (%)**	**R**
1	8.12±2.49	0.04±0.01	100.00±0	-*	69.07 ±1.07	0.51±0.02	99.99±0	5.16±0.13
3	25.50±12.20	0.13±0.07	99.99±0.01		69.01±36.92	0.73±0.53	99.97±0.01	3.60±0.15
5	99.59±0.14	2.90±0.32	-	-	97.07±2.63	1.64±0.32	-	-

*****at 100% of inhibition the equation for the calculation of R (Eq. 4) presents limitations

Figure 1.- Rheological behavior of a) PDLLA solutions at 0, 1, 3 and 5 wt. % of n-ZnO and b) PHB solutions at 0, 1 and 3 wt. % of n-ZnO.

Figure 2.- SEM images of PDLLA fibrous material at 1 wt. % (a and b), 3 wt. % (d and e) and 5 wt. % (g and h) of n-ZnO, box charts of fiber diameters and porosities (Ø) (c, f and i).

Figure 3.- SEM images (a, d and g), elemental mapping of zinc (b, e and h) and TEM images (c, f and i) of PDLLA fibrous material at 1 wt. % (a, b and c), 3 wt. % (d, e and f) and 5 wt. % (g, h and i) of n-ZnO (images obtained by SEM-EDS).

Figure 4.- SEM images of PHB fibrous material at 1 wt. % (a and b) and 3 wt. % (d and e) of n-ZnO, box charts of fiber diameters and porosities (Ø) (c and f).

Figure 5.- SEM images (a and d), elemental mapping of zinc (b and e) and TEM images (c and f) of PHB fibrous material at 1 wt. % (upper images) and 3 wt. % (bottom images) of n-ZnO (images obtained by SEM-EDS).

Figure 6.- Degradation patterns derived from TGA of the centrifugally spun PDLLA fibers (a) and PHB fibers (b) obtained at different concentrations of n-ZnO.

Figure 7.- DSC thermograms derived from one cycle of heating-cooling-heating of a) PDLLA and b) PHB fibrous mats at different concentration of n-ZnO.

Figure 8.- Young's modulus (E) and tensile strength (σ) of the materials obtained with PDLLA (a) and PHB (b) at different concentrations of n-ZnO.

Figure 9.- Osteoblast cell viability evaluated after 1, 3, 5 and 7 days with resazurin for PDLLA (a) and PHB (b). A statistical analysis is shown measuring the standard deviation of the mean, n= 3 trial experiment (* $p < 0.05$, ** $p < 0.01$).

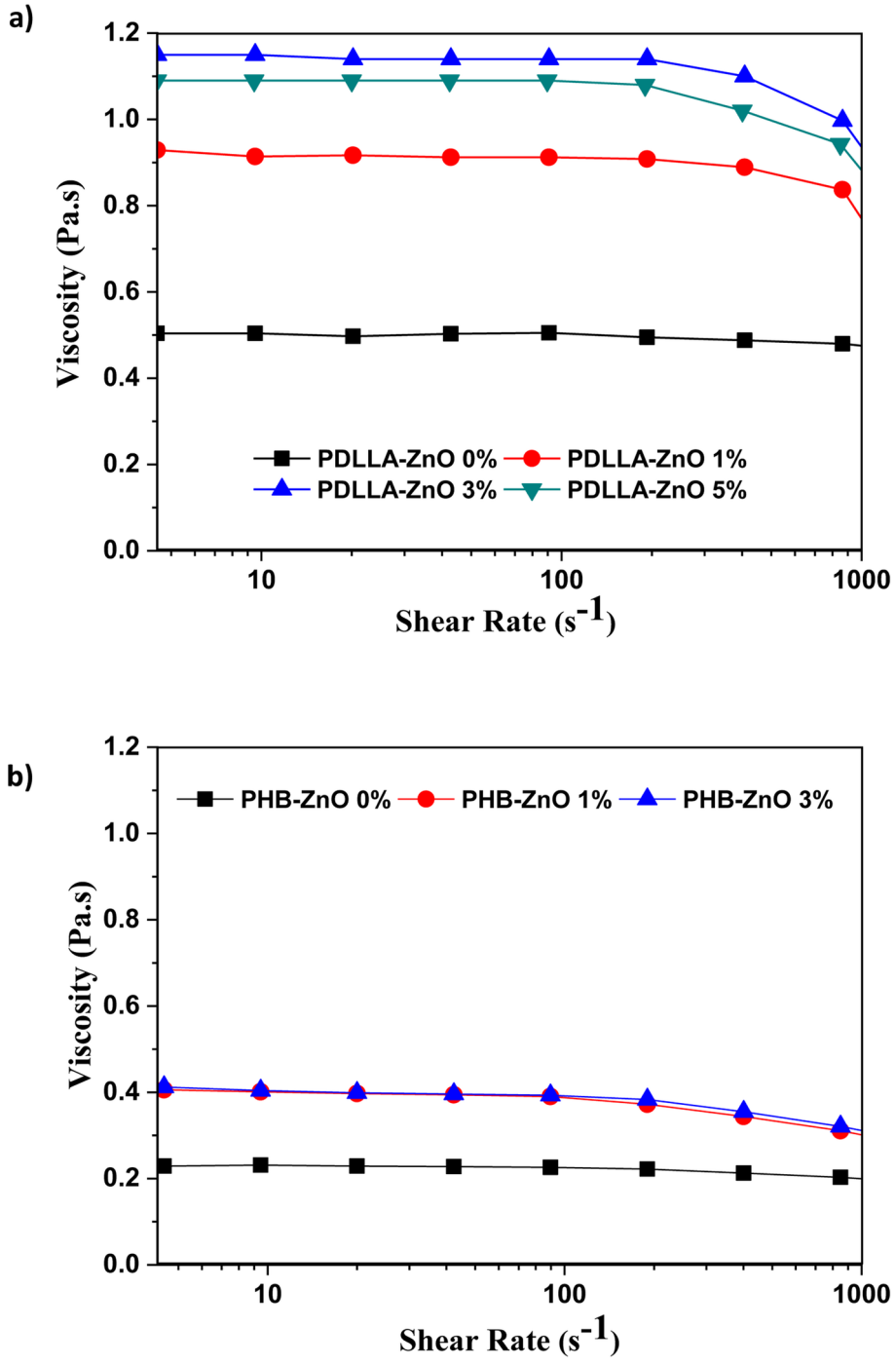

PAT_4987_Fig 1.tif

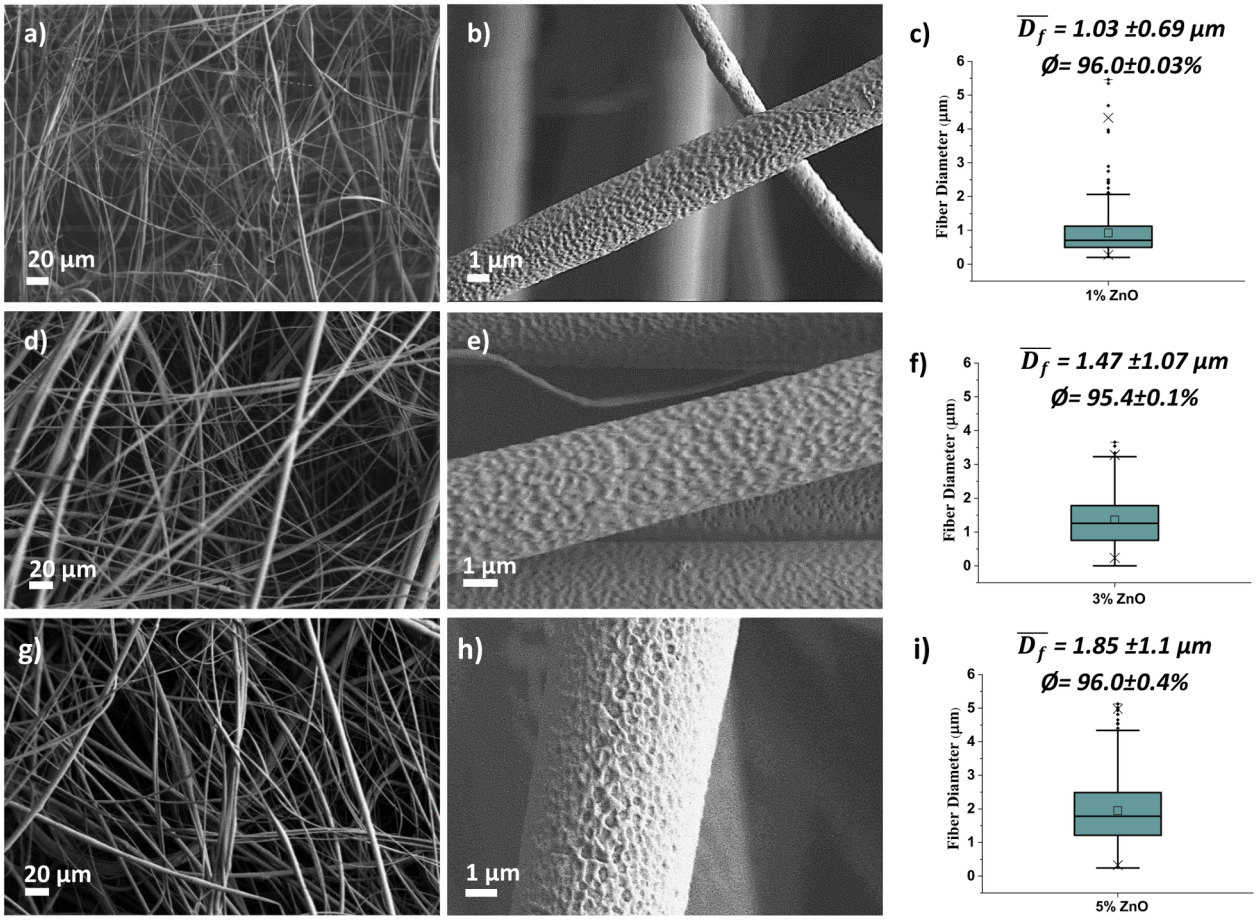

PAT_4987_Fig 2.tif

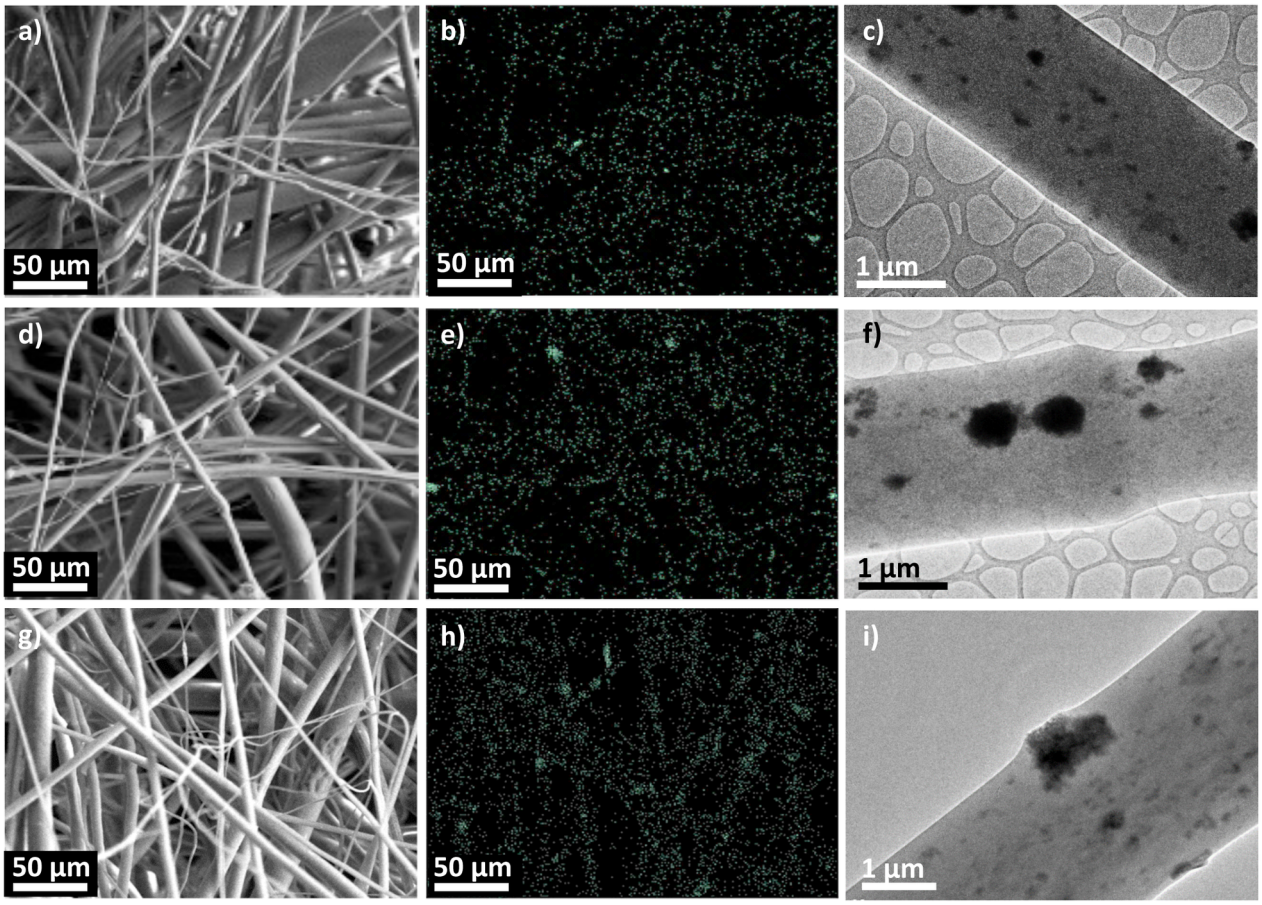

PAT_4987_Fig 3.tif

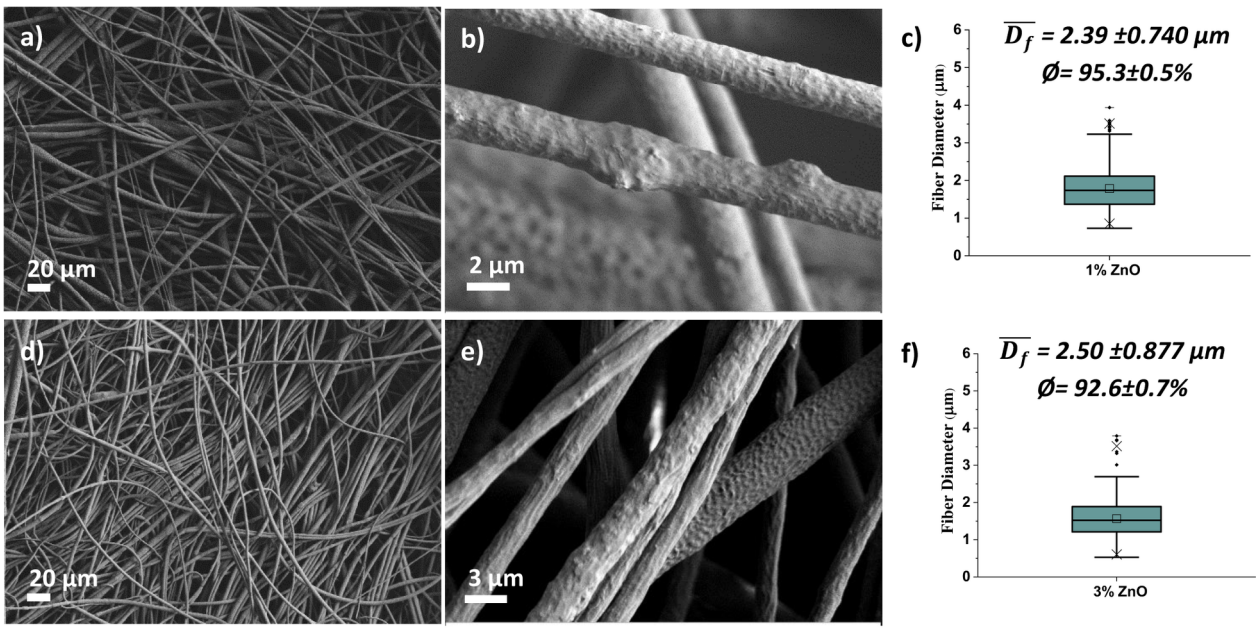

PAT_4987_Fig 4.tif

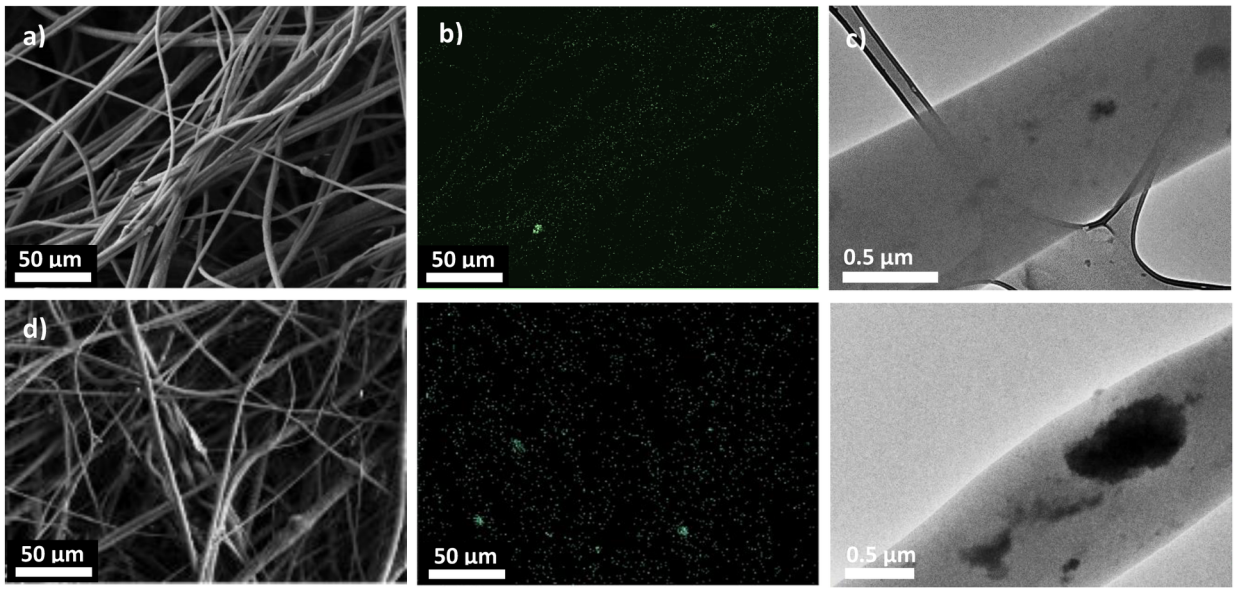

PAT_4987_Fig 5.tif

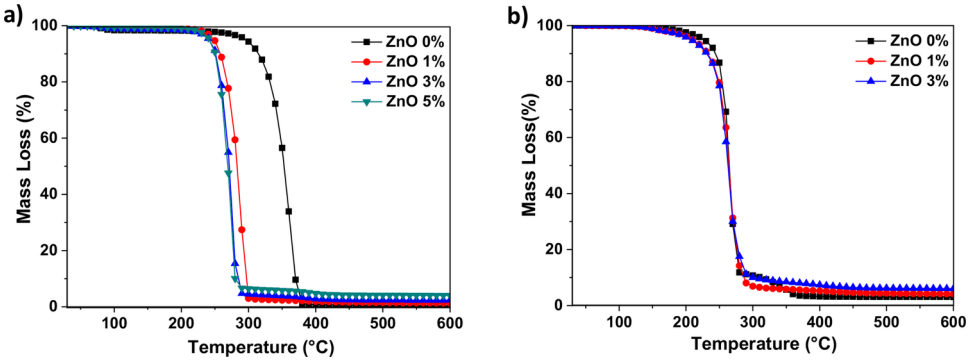

PAT_4987_Fig 6.tif

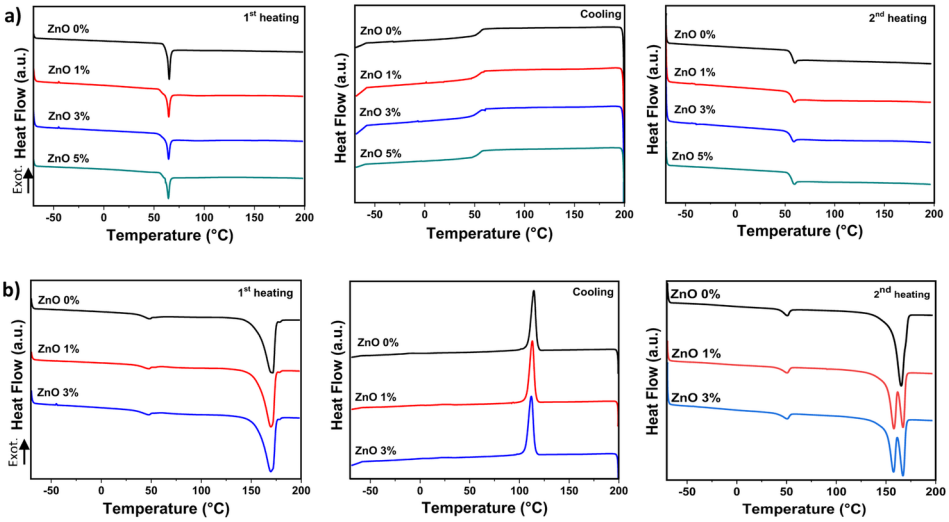

PAT_4987_Fig 7.tif

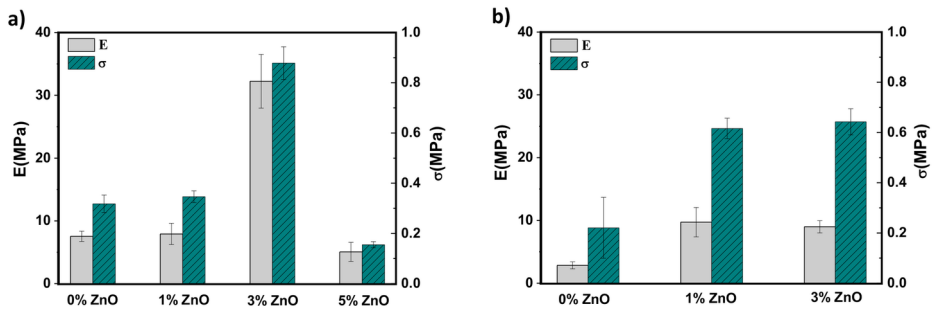

PAT_4987_Fig 8.tif

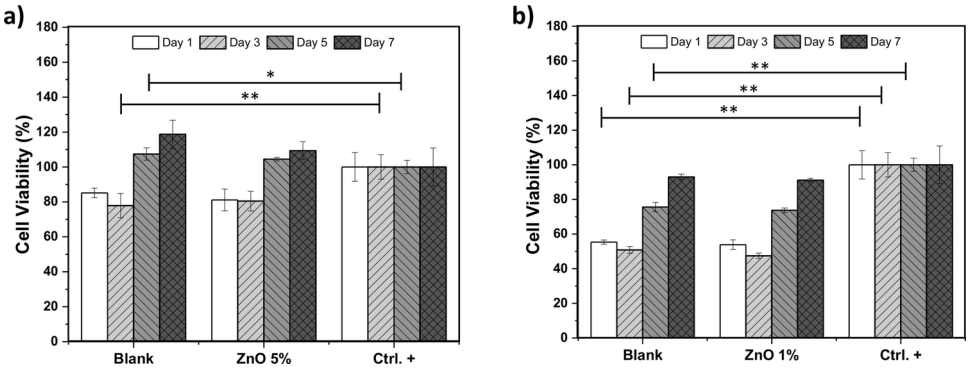

PAT_4987_Fig 9.tif